Available online at www.sciencedirect.com
SCIENCE DIRECT®
Physica A 352 (2005) 171–201
PHYSICA A
www.elsevier.com/locate/physa

Physics of cell elasticity, shape and adhesion

S.A. Safran[a,*], N. Gov[b], A. Nicolas[c], U.S. Schwarz[d], T. Tlusty[a]

[a]Department of Materials and Interfaces, Weizmann Institute of Science, Rehovot 76100, Israel
[b]Department of Chemical Physics, Weizmann Institute of Science, Rehovot 76100, Israel
[c]Centre de Recherche Paul Pascal, 33600 Pessac, France
[d]MPI of Colloids and Interfaces, 14424 Potsdam, Germany

Available online 12 January 2005

Abstract

We review recent theoretical work that analyzes experimental measurements of the shape, fluctuations and adhesion properties of biological cells. Particular emphasis is placed on the role of the cytoskeleton and cell elasticity and we contrast the shape and adhesion of elastic cells with fluid-filled vesicles. In red blood cells (RBC), the cytoskeleton consists of a two-dimensional network of spectrin proteins. Our analysis of the wavevector and frequency dependence of the fluctuation spectrum of RBC indicates that the spectrin network acts as a confining potential that reduces the fluctuations of the lipid bilayer membrane. However, since the cytoskeleton is only sparsely connected to the bilayer, one cannot regard the composite cytoskeleton–membrane as a polymerized object with a shear modulus. The sensitivity of RBC fluctuations and shapes to ATP concentration may reflect topological defects induced in the cytoskeleton network by ATP. The shapes of cells that adhere to a substrate are strongly determined by the cytoskeletal elasticity that can be varied experimentally by drugs that depolymerize the cytoskeleton. This leads to a tension-driven retraction of the cell body and a pearling instability of the resulting ray-like protrusions. Recent experiments have shown that adhering cells exert polarized forces on substrates. The interactions of such "force dipoles" in either bulk gels or on surfaces can be used to predict the nature of self-assembly of cell aggregates and may be important in the formation of artificial tissues. Finally, we note that cell adhesion strongly depends on the forces exerted on the adhesion sites by the tension of the cytoskeleton. The size and shape of the adhesion regions are strongly modified as the tension is varied and we present an elastic model that relates this tension to deformations that induce the recruitment of new molecules to the adhesion region. In all these examples, cell shape and

*Corresponding author. Tel.: +972 89343362; fax: +972 89344138.
E-mail address: sam.safran@weizmann.ac.il (S.A. Safran).

0378-4371/$ - see front matter
doi:10.1016/j.physa.2004.12.035

adhesion differ from vesicle shape and adhesion due to the presence of the elastic cytoskeleton and to the fact that active processes (ATP, molecular motors) within the cell modify cytoskeletal elasticity and tension.

Keywords: Elasticity; Membrane; Adhesion

1. Introduction

Biological cells must fulfill a complex and dynamically changing set of requirements in order to survive, function and reproduce. For example, red blood cells (RBC) must adapt to the relatively wide range of capillary sizes found in blood vessels; they must be at the same time deformable while maintaining their cellular integrity and function. Epithelial cells that form tissues that cover the internal and external surfaces of organs (e.g., skin cells, lining of the lungs, intestines) must adhere to substrates and to each other under a wide variety of circumstances; their adhesion properties can be regulated by the cell which simultaneously senses the chemical and mechanical properties of its environment. Fibroblasts that maintain connective tissue and play an important role in wound healing have their own internal mechanisms for regulating the elastic forces that they exert. While the structure and physical properties of biological cells must ultimately be described by the known laws of chemistry and physics, there are important differences between conventional "dead" materials and living matter. Even if one focuses (as does this article) on the physical structure and dynamics of cellular components and not on the more complex problem of genetics and development, it is necessary to consider and to account for cell function when describing cell structure. This distinguishes "live" matter from the usual systems treated by materials physics.

In this review, we summarize recent theoretical progress that relates the physics of cell elasticity to cell structure, function and adhesion. From the point of view of materials physics, biological cells have some common features with artificial "soap bubbles" or other self-assembled amphiphilic systems [1]; both are characterized by a membrane that isolates the contents from the environment. However, in contrast to swollen micelles, microemulsions and vesicles—systems that have been intensively investigated both theoretically and experimentally using the tools and concepts of soft matter physics—the cytoplasm of the cell is not a simple fluid. The interior of cells contains the cytoskeleton, an elastic gel composed of crosslinked, long-chain protein molecules; this gives the cell shear rigidity and shape integrity. In most cells, the cytoskeleton [2] is composed of several components, including actin, microtubules and intermediate filaments, each of which have different elastic properties [3] that can be used by the cell in a variety of circumstances. As mentioned above, the cell can regulate its elasticity by varying the self-assembly of the macromolecules that form the cytoskeleton. In addition, the cytoskeleton can exert forces on the cellular environment; this is important in the regulation of adhesion. Force generation that leads to tension in the actin network arises from the action of

myosin molecular motors that are activated by ATP to change conformation and exert forces on the actin filaments.

Recent experiments [4,5] show that, in contrast to artificial vesicles that exert only normal forces when adhering to a substrate, adhering cells show both normal and lateral forces. The normal forces arise from the action of either specific adhesion molecules or non-specific interactions (e.g., van der Waals interactions or macromolecular adsorption) while the lateral forces arise from elastic deformations of the adhesion region by cytoskeletal forces. These lateral forces regulate the size and shape of the finite-sized, discrete adhesion regions (in some cases called focal adhesions (FA)) [5] and allow a cell to probe and to adjust the strength of the adhesion to its physical environment. FA are large (micron-sized), discrete cell-matrix adhesion regions that contain transmembrane adhesion receptors of the integrin protein family. For mechanically active cells like fibroblasts with mature FA, there could be hundreds of FA distributed mainly along the cell rim; the forces associated with these FA keep the cell under tension. The physical origin of the mechanosensor in the cell and the conversion of elastic information to a biochemical response that recruits additional proteins to the adhesion region is an important problem in cell biology today [5].

These forces that arise from the tension in the actin cytoskeleton tend to polarize the tense actin filaments that in this context are termed stress fibers. Thus, one can sum over all the local FA and, in a coarse-grained picture, model such an adhering cell as a pair of nearly equal and oppositely directed contraction forces (termed an elastic force dipole) with typical forces of 100 nN over a scale of tens of microns. For stationary cells, Newton's law implies that the vector sum of all the forces must vanish and the dominant remaining forces will be dipolar in nature. Due to the anisotropic nature of the actin fibers of the mechanically active, cellular cytoskeleton, the force dipoles are themselves anisotropic. An interesting physics problem [6,7] concerns the interactions and self-assembly of many such force dipoles; this corresponds to the interactions of many cells, each of which adheres to an elastic medium such as a substrate or in a three-dimensional gel. These dipoles interact via the elastic deformations of the medium, and can form chains or other self-assembled structures. Because these interactions are long-range, the details depends on the boundary conditions and sample shape. In addition, the interaction strength depends on the elasticity of the substrate as well as on its deformations: for example, cells have been observed to migrate toward stiffer substrates and to rotate on elastically strained media [8]. The physics of cell adhesion and the interactions of cells in elastic media are important for the understanding of tissue formation and engineering [9] as well as wound healing and metastasis.

At the level of the individual cell, the competition of adhesion forces and the tension and bending properties of the bilayer membrane determine the shapes of adhering cells. Here again, the cytoskeletal elasticity plays a role and makes this problem different from the adhesion of artificial vesicles. In particular, the shear modulus of the cell contributes to the line tension at the cell–substrate interface. Analysis of measurements of the shape of adhering cells as a function of the cytoskeletal elasticity explained the observations [10] of an interesting shape

transition in cells that were treated with a drug that depolymerized (and thus reduced the elasticity of) the actin cytoskeleton. The resulting sun-like structure of the cell then showed a further pearling instability in which the characteristic wavelength depends on the cytoskeletal elastic modulus.

The coupling between the elastic cytoskeleton and the fluid, lipid membrane is important for understanding the mechanical properties and fluctuation spectrum of the cell [12,13]. The details of the cytoskeleton components and their geometry vary between cells, but there are general features that are common to all: the fluid bilayer is attached to the cytoskeleton through specialized [14] membrane proteins, confined to small attachment patches of ~ 10–$50\,\mathrm{nm}$ each, that can be relatively sparse ($\sim 100\,\mathrm{nm}$ apart in the RBC [11]). The cytoskeleton, that can either be a three-dimensional actin gel that fills the entire cell volume or a thin, quasi-two-dimensional protein network as in RBC, is usually much stiffer than the bilayer, and its gel-like structure gives it a shear modulus. The fluctuations of that part of the bilayer that is attached to the cytoskeleton are therefore confined in the normal and lateral directions. It is interesting to see how this highly inhomogeneous potential affects the entire membrane, including those sections that are not directly attached to the cytoskeleton.

RBC have a two-dimensional cytoskeleton composed of an approximately hexagonal network of crosslinked, spectrin protein molecules. Measurements of the thermal fluctuations of the cell membrane result in amplitudes much larger than one would expect [1,15–17] if one would attribute the full shear modulus of the spectrin network to the bilayer membrane. Increasing the shear modulus of the spectrin network by the addition of additional crosslinking agents has a negligible effect on the observed fluctuation amplitudes [17]. Recent models of RBC fluctuations [12,13,18] showed that the sparse nature of the coupling of the two-dimensional cytoskeleton of RBC to the membrane allows significantly larger membrane fluctuations. The cytoskeleton results in an effective membrane tension [12,13,19] as well as a soft potential that confines the membrane fluctuations. Again, in contrast to ''dead matter'', the cytoskeletal elasticity is regulated by ATP that can change the nature of the actin–spectrin crosslinks. Defects in the cytoskeleton induced by ATP may explain the increase in fluctuations as the amount of ATP in RBC is increased [18,20]. Other cytoskeletal elastic effects that determine RBC shape include the formation of fold-lines [18,21] in RBC that are confined to narrow capillaries and to changes in the overall RBC shape [22–24] (echinocyte or discocyte formation). These effects are controlled by ATP thus indicating how non-equilibrium processes are critical in determining even the steady-state shape of biological cells.

This review begins in the next section with a discussion of the elasticity of the two-dimensional spectrin network of RBC and its implications for the static and dynamic fluctuations of RBC. The theoretical predictions are compared with experiments that determine the magnitude of the effective tension and confining potential induced by the cytoskeleton. The observed increase of the fluctuations with ATP activity and the release of ATP by deformed RBC is discussed in terms of cytoskeletal defects induced by ATP.

In Section 3, the effects of the three-dimensional actin network on the shapes of adhering cells is discussed. The shape instabilities observed as the cytoskeleton shear modulus is reduced by the addition of a drug can be quantified and used as a measure of the integrity of the cytoskeletal network elasticity.

Section 4 reviews the results of an analysis of experimental data that determines the forces exerted by the stress fibers of adhering cells. The cells can be characterized as "force dipoles" whose interactions determine the nature of the self-assembly of cells on substrates in three-dimensional gels.

A model for the origin of the mechanosensitivity of adhering cells is reviewed in Section 5 in light of experiments that measured the size and shape dependence of cellular FA on external forces exerted on the cytoskeleton. It is suggested that the deformations induced in the adhesion region by the stress fibers that are under tension due to the actomyosin activity in the cytoskeleton can give rise to a biochemical response in which additional proteins are recruited to the adhesion zone.

2. Elasticity of RBC

The shape of RBC is strongly determined by the mechanical properties of the cytoskeleton and by ATP activity. The surface of the RBC is a composite material containing an outer lipid bilayer and an inner, two-dimensional cytoskeleton that is composed of the protein spectrin [11] attached in a sparse manner to the lipid bilayer [12,13]. The links of the network consist of flexible spectrin molecules ($R \sim 80$–100 nm), crosslinked at the network nodes by a complex containing a short (~ 30 nm) actin filament, band-4.1 and other proteins [11,14]. We begin with a discussion of the cytoskeleton effects on the shape fluctuations of RBC and then consider the role of ATP in enhancing the fluctuations as well as shape changes.

2.1. Shape fluctuations

In this section, we focus on the effects of the inhomogeneous potential of the spectrin network on the thermal fluctuations of the membrane. These fluctuations have been measured in RBC [15], and the effective membrane bending modulus κ was found to vary dramatically as a function of the measured wavevector q. These observations, as well as that of the temporal spectrum [20], have presented a theoretical challenge since they appear to indicate that the bilayer behaves as if it is almost detached from the underlying cytoskeleton [12,16]. At the same time, the membrane acquires a wavelength-dependent surface tension, in addition to its curvature modulus [12,13]. This tension is much larger than estimated from the finite size effect [1] $\sigma \gg \kappa/R^2$. We have found that we can predict these properties using a simple, well-controlled model.

The simplest description of the membrane neglects the thickness of the cytoskeleton and the sparse attachments to the bilayer, and treats a bilayer that is completely attached to a two-dimensional (i.e., zero thickness) cytoskeleton [15,16]. In this case, the membrane has, at all length scales, the bare bending modulus of the

bilayer and the shear modulus of the cytoskeleton which is of the order of $6 \times 10^{-6}\,\mathrm{J/m^2}$ [25]. This would be expected to show very small thermal fluctuations due to the large shear restoring force. However, this model is ruled out by the observed distribution of the fluctuation amplitude among different shape modes and over the RBC surface [15,16]. We therefore must take into account the relatively weak coupling between the bilayer and cytoskeleton, due to the sparse connections and the soft nature of the cytoskeleton shell.

Our model that accounts for the relatively large amplitude of RBC fluctuations describes the relatively weak potential exerted on the membrane by the soft cytoskeletal shell, that is sparsely attached to the bilayer. The average bilayer–shell distance is related to the observed amplitude of thermal fluctuations, and depends on the undulations of both the bilayer and spectrin filaments. The spectrin filaments form a connected, quasi-two-dimensional shell that has a three-dimensional thickness of $d \sim 30\,\mathrm{nm}$, due to the conformations of the soft filaments out of the plane of the shell. This can be modeled by a restoring force on the bilayer, which we account for via a harmonic potential. The force acts at all bilayer–spectrin distances due to relatively delocalized and "soft" nature of the spectrin network. Additionally, the sparse attachment points of the membrane to this potential induce an effective surface tension in the bilayer [13]. The resulting free energy is therefore given by [12]

$$F \simeq \int \mathrm{d}S \left[\frac{1}{2}\,\sigma(\nabla h)^2 + \frac{1}{2}\,\kappa(\nabla^2 h)^2 + \frac{1}{2}\,\gamma h^2 \right], \tag{1}$$

where σ is the effective surface tension and γ describes the confining harmonic potential. The spectrin filaments behave as entropic springs; they can have random conformations in the half-space beneath the lipid bilayer, since they are not strongly adsorbed to the bilayer, except at their ends [26]. This would predict a fluctuation amplitude given by

$$\langle h_q^2 \rangle = \frac{k_B T}{\kappa_q q^4}\,, \tag{2}$$

where κ_q is a renormalized bending modulus given by

$$\kappa/\kappa_q = \frac{\kappa}{\kappa + \sigma q^{-2} + \gamma q^{-4}}\,, \tag{3}$$

where the bare bending modulus $\kappa \sim 2 \times 10^{-20}\,\mathrm{J}$.

We now analyze the static fluctuation spectrum, that is the height fluctuations as a function of the wavevector q [27]. In the limit of short wavelengths (large q) we find that the data for the mean-square amplitude is reasonably described by the expression for a free membrane: $\langle h_q^2 \rangle = k_B T/(\kappa q^4)$ with a bare bending modulus $\kappa \sim 2 \times 10^{-20}\,\mathrm{J}$. At the largest wavevectors, the data are noisy due to experimental limitations. We view this value of κ as indicative of the bare value of the bending modulus of the bilayer, since in this limit, the bilayer is largely free of the sparse cytoskeleton connections. The amplitude of fluctuations is also small compared with the average bilayer–cytoskeleton distance of $d \sim 30\,\mathrm{nm}$, so that interaction between the two is small.

In the other limit of small wavevectors, we find that the fluctuation amplitude saturates. In order to find the value of the parameters γ and σ, we plot in Fig. 1 the renormalized effective bending modulus κ_q (Eq. (3)). Using this plot, we find the ratio γ/κ. Fitting the data, we get the following values for the small q range: $\gamma \sim 1-8 \times 10^7\,\mathrm{J/m^4}$ and $\sigma \sim 5-12 \times 10^{-7}\,\mathrm{J/m^2}$, where the variability represents the natural spread of values among different cells. Using these values to fit the experimental data for the *absolute* amplitude of the static fluctuations [18], we find that it is enhanced by a factor of ~ 3, which we attribute to an increased effective temperature $T_{eff}/T \sim 3$ due to the ATP-driven height fluctuations. Note that exactly the same enhancement factor explains the measurements of the *dynamic* fluctuation amplitude in ATP-depleted and ATP-containing RBC ghosts (in very different experiments) [13,20], showing the overall consistency of our description.

For comparison, we compare the data for the stomatocyte cell [27]. These cells are known to have a weakened cytoskeleton and a much expanded bilayer [24]. The first effect is taken into account by a reduction of the surface tension σ and γ by $\sim 15\%$, since both are linearly dependent on the shear modulus of the cytoskeleton μ [13],

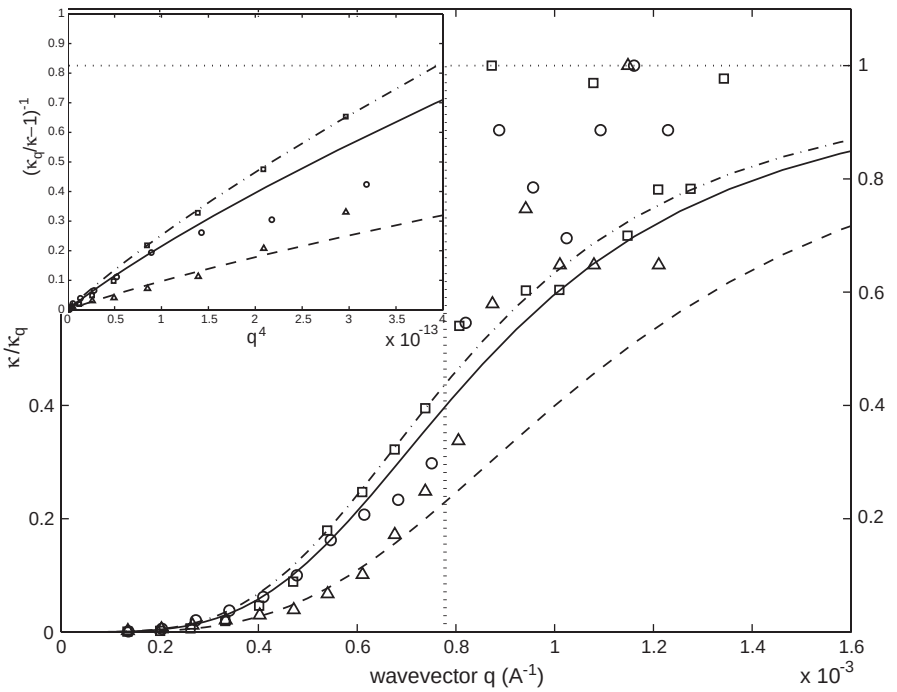

Fig. 1. Calculated normalized effective bending modulus κ_q (Eq. (3)) compared with the experimental data [27]: normal cells—circles (solid line), stomatocyte—squares (dashed-dot line), echinocyte—triangles (dashed line). The vertical dotted line shows the crossover wavevector $q_0 \sim (\gamma/\kappa)^{1/4}$. The inset shows the same data in the limit of small q's, to determine the ratio γ/κ. The linearity in this plot at small values of q indicates that the value of γ (arising from the cytoskeletal potential) must be non-zero.

which is reduced by this amount. The weaker cytoskeleton allows the bilayer to have a shape transition into a stomatocyte, that is characterized by a stretched bilayer [24]. In this case, ATP-induced defects in the cytoskeleton do not translate into normal motion of the bilayer, and the effective temperature is therefore found to be $T_{eff}/T \sim 1.2$.

The data for the echinocyte cell [27] fits with our expectation of increased surface tension and harmonic potential parameters by a factor of ~ 2.2, compared to the values for the normal RBC. We also expect the effective temperature to be essentially given by its bare, thermal value, since ATP activity is absent in the cytoskeleton of the echinocyte. Indeed, measurements of the effective absolute fluctuation amplitude are found to be ~ 3.8 times smaller than for the normal RBC.

An extension of the static theory to treat the dynamical fluctuations has been presented in Refs. [12,28,29]; for the hydrodynamic analysis, the cytoskeleton can be taken to be a somewhat permeable wall that impedes the water flow; this is in addition to its role as a source of membrane tension and a confining potential. We note that our analysis of the *dynamic* fluctuation data is consistent with an effective value of the average bilayer–cytoskeleton distance, $d \sim 30\,\text{nm}$, which is determined by the soft potential strength, γ, deduced from our analysis of the *static* fluctuation data. The slow water flow appropriate to the measurements of the low frequencies of dynamic bilayer fluctuations is such that the cytoskeleton is nearly impermeable. This is because on the slow time scale of the water flow, the spectrin network fluctuates and effectively covers the entire two-dimensional plane. The transient, ATP-induced defects are much faster than these slow flows, so that the water is bounded on one side by the bilayer and on the other side by the spectrin network [12] which on average is at a distance d from the bilayer. Since the restoring force is constant, the ATP activity is best taken into account through an increased effective temperature, i.e., increased agitation force.

2.2. Microscopic model

The phenomenological analysis presented above found that the sparse coupling of the cytoskeleton and the RBC membrane results in a description of a membrane characterized by three effective parameters κ, σ, γ. In Ref. [13], we presented a microscopic model of a bilayer membrane in a periodic potential and showed that the phenomenological parameters, κ, σ, γ, have their origin in the long-wavelength limit of that microscopic model. The phenomenological parameters are shown to be related to the amplitude and wavelength of the potential that the cytoskeleton exerts on the membrane.

Our simplified microscopic model approximates the membrane cytoskeleton coupling as a periodic harmonic potential. The point of attachment of the cytoskeleton to the membrane is through relatively short and rigid protein complexes [2,11] (e.g., p4.1, p55). The *flexible* spectrin filaments provide the smooth restoring force of the cytoskeleton that acts on the membrane and this motivates our harmonic approximation. The spectrin molecules behave as linear entropic springs, with non-linearity at large extensions [30], beyond the range of the thermal fluctuations

discussed here. We studied [13] two extreme situations for the lateral potential: a series of delta functions and a smooth sinusoidal function.

The Hamiltonian H of the membrane is written as

$$H = \int \mathrm{d}\vec{r}\left[\frac{\kappa}{2}(\nabla^2 h)^2 + \int \mathrm{d}\vec{r}' V(\vec{r}-\vec{r}')h(\vec{r})h(\vec{r}')\right], \tag{4}$$

where κ is the bending modulus and $V(\vec{r}-\vec{r}')$ is the external potential that represents the inhomogeneous coupling to the cytoskeleton. For a localized, harmonic confining potential, the second term in Eq. (4) becomes $V(\vec{r})h(\vec{r})^2$. To calculate the correlations, we use a relation between the linear response of the membrane to a localized force, $f\delta(\vec{r})$, and the correlation function for membrane fluctuations [1,13]. The real-space correlation function $\langle h(\vec{r})h(0)\rangle$ is related to the function $\chi(\vec{r})$ determined by the differential equation

$$V(\vec{r})\chi(\vec{r}) + \kappa\nabla^4\chi(\vec{r}) = f\delta(\vec{r})\,. \tag{5}$$

In Ref. [13] this equation is solved analytically for the case of a two-dimensional checkerboard potential characterized by a spatial variation proportional to $V_0\cos(Gx)\cos(Gy)$ with the single wavevector $\vec{G}$. The approximation used neglects the coupling to higher harmonics and predicts an effective bending stiffness $\overline{\kappa}$, effective tension $\overline{\sigma}$ and effective potential $\overline{\gamma}$ from an expansion of the height correlation function to fourth order in wavevector. In the limit of both weak ($V_0/G^4\kappa \ll 1$) and strong ($V_0/G^4\kappa \gg 1$) confinement, we have

$$V_0 \to 0 : \overline{\gamma} \to V_0, \quad \overline{\sigma} \to -\frac{V_0^2}{8G^6\kappa}, \quad \overline{\kappa} \to \kappa\,,$$

$$V_0 \to \infty : \overline{\gamma} \to \frac{3V_0}{4}, \quad \overline{\sigma} \to 2\kappa G^2, \quad \overline{\kappa} \to \frac{5}{4}\kappa\,. \tag{6}$$

For weak confinement, both the curvature modulus and the confinement potential γ are easily understood; however, we find a surprising, effective *negative* surface tension for weak potentials $V_0 < 4\kappa G^4$. In the limit of strong confinement, we find that the surface tension saturates to a positive value that is much larger than the tension due to finite size effects, with a somewhat renormalized bending modulus and monotonically increasing uniform confinement. The analytical approximation compares well with a numerical solution for long-wavelength modulations (small values of $\vec{G}$) or small modulation amplitudes.

For both small and large values of $\vec{G}$, it is the "pulling" effect of the inhomogeneous pinning that induces the appearance of the effective surface tension. In the limit of $V_0 \to \infty$, the clamping has an effect that is similar to that of positive tension, σ, and the fluctuations are reduced. In the limit $V_0 \to 0$, there appears a wavevector q_0, at which the correlations are maximal; this is similar to the effect of buckling that a negative tension would induce.

Comparing Ref. [13] with the fits to the static scattering experiments in RBC, we find in both cases that the predicted surface tension $\overline{\sigma} \sim 2 \times 10^{-7}\,\mathrm{J/m^2}$ is smaller than the measured value by a factor of ~ 3. The calculated surface tension is close to

the asymptotic value of strong confinement $\overline{\sigma} \sim 2\kappa G^2$ (see Eq. (6)). Note also that the experimental value is about 30 times smaller than the cytoskeletal shear modulus ($\mu \sim 6 \times 10^{-6}\,\mathrm{J/m^2}$), while much larger than the surface tension arising from area conservation of the RBC [12]: $\sigma_0 = \kappa/R^2 \sim 1 \times 10^{-9}\,\mathrm{J/m^2}$ (taking $R \sim 4\,\mu\mathrm{m}$ for the RBC radius). The surface tension imposed by the periodic potential is therefore distinct from both the cytoskeleton shear strength and the area conservation condition.

We now relate the values of the model parameters G and V_0 to the microscopic structure of the RBC cytoskeleton. The calculated periodicity is of the order of the observed average distance between cytoskeleton and bilayer connection sites [15] ($\sim 150\,\mathrm{nm}$). Additionally, the values of the peak confining harmonic potential exerted by the cytoskeleton $V_0 \sim 100\kappa G^4$ can be related to the shear strength per unit area of the cytoskeleton μ: $V_0 \sim \mu G^2 \simeq 0.14\text{–}0.4 \times 10^8\,\mathrm{J/m^4}$. The strength of the confining that the cytoskeleton exerts on the lipid membrane at the coupling site is related to the cytoskeleton stiffness. This is because it is only the local shape changes of the cytoskeleton that provide a restoring force to the fluctuations of the lipid membrane, in addition to the intrinsic bending modulus of the bilayer.

Comparing the behavior of the model with the experiments as a function of wavevector, we find that the two-dimensional sinusoidal checkerboard potential can reproduce fairly well the low q behavior, including the appearance of the relatively large effective surface tension. The measured data, though, shows a more abrupt change [19] around the crossover wavevector q_c (see Fig. 4 of Ref. [13]).

Although the coupling of the cytoskeleton to the membrane occurs at distinct sites, the checkerboard model gives a surprisingly good approximation of the real cytoskeleton–bilayer coupling in the RBC, because of the diffusion-induced fluctuations of these coupling points in the fluid, bilayer membrane. This is probably because the actual potential is smoothed by the fluctuations of the spectrin molecules and of the finite size patches that connect them to the membrane.

2.3. Activity and structure

In the absence of ATP, such as in depleted cells or washed ghosts [20], the r.m.s. amplitude at a given point in space of the bilayer thermal fluctuations (alone) is $\overline{h}_{ther} \sim 30\,\mathrm{nm}$. When ATP is added, the fluctuation amplitude rises and saturates at physiological concentrations, giving $\overline{h} \sim 80\,\mathrm{nm}$. In the previous discussion of the phenomenological model [12], we have shown that a consistent description of both the static and dynamic data is possible if we treat the ATP effect as introducing a higher effective temperature $T_{eff}/T \sim 3$. We now consider the origin of this effect.

The consumption of ATP is known to induce large membrane fluctuations [12,20]. Since the hydrolysis of ATP releases $\Delta E_{atp} \sim 13 k_B T$, it provides more than enough energy to dissociate the spectrin from the actin at the nodes of the network; that energy cost is only $\Delta E_{sa} \sim 7 k_B T$. The rate of energy transfer by this mechanism into shape fluctuations of the membrane is limited by the following quantities: the elastic energy released in the membrane, the concentration of ATP and the time it takes for the membrane to dissipate this energy and "re-attach" to the cytoskeleton. The

ATP-induced dissociations of spectrin are transient, because the dissociated spectrin can re-associate with the actin filament.

The adsorption of ATP to the phosphorylation sites at the spectrin–actin junctions can be described by the equilibrium occupation probability; this assumes that the ATP in the cytoplasm can be treated as a reservoir with concentration n_{ATP}. Standard thermodynamics gives

$$n_d = \frac{n_{ATP} e^{\varepsilon}}{1 + n_{ATP} e^{\varepsilon}} , \tag{7}$$

where ε (in units of $k_B T$) is the energy to preferentially adsorb at the spectrin–actin sites as opposed to anywhere else on the membrane surface, and is given by the following balance:

$$\begin{aligned} \varepsilon &\simeq (\Delta E_{atp} - \Delta E_{sa} - k_B S_f - \Delta E)/(k_B T) \\ &\simeq 13 - 7 + 1.5 + 1.5 \simeq 9 , \end{aligned} \tag{8}$$

where S_f is the entropy change due to the release of the spectrin filament. The last term in Eq. (8) represents the mechanical energy released by the spectrin dissociation, estimated as $\Delta E \simeq \mu(R - R_0)^2 \simeq 1.5 k_B T$, where μ is the cytoskeletal shear modulus, $R \sim 80$–100 nm is the typical spectrin network spacing and $R_0 \sim 70$ nm is the ideal spectrin distance in the absence of the bilayer [18]. Due to the large adsorption energy, the ATP occupation of the spectrin–actin sites is saturated at relatively low ATP concentrations, in agreement with experimental data [20]. Dissociation of the actin–spectrin complex means that on both sides of the dissociated spectrin there are now five-fold nodes that tend to buckle upwards [31] and can exert a force on the membrane. Thus, ATP-induced spectrin dissociation converts the stored elastic energy of the filament into normal motion of the membrane. In addition, the dissociation can affect the membrane–cytoskeleton coupling proteins; this would also tend to increase the membrane fluctuations.

When the energy released by spectrin dissociation is added to the thermal energy $k_B T$ that is dissipated by each membrane mode, one predicts [12] an enhanced effective temperature of the order of the measured factor of $T_{eff}/T \sim 3$. Our estimate is valid under the condition that the ATP-induced processes, similar to the thermal motion of the membrane, are spatially incoherent. However, on the length scale of the cytoskeleton network (~ 200 nm) itself, the motion is not thermal and does not satisfy the fluctuation-dissipation theorem [32]. The use of an effective temperature is only correct at larger scales where non-linear couplings mix the energy of the discrete motion into membrane modes of longer wavelength.

The local transfer of energy from the ATP to the membrane motion, on the scale of a single network element, can be estimated from the equation of motion for the local amplitude h of the membrane fluctuations (in the usual limit of large damping)

$$\dot{h(t)} + \omega_m h = \xi(t) , \tag{9}$$

where a^2 is the area of the membrane contained in one network triangle (the mesh size of the spectrin network: $a \sim 80$ nm), η is the viscosity of the surrounding fluid

and $\xi(t)$ is the normalized force, given by $\xi(t) = F(t)/(4a^2\eta k)$, where $k \sim 1/a$ and $F(t)$ is the actual force on the membrane that comes from the ATP-included disconnections of the spectrin chains from the network or of the spectrin–membrane coupling. For disconnections of the spectrin network, the force is derived from the energy ΔE discussed after Eq. (8). The first term on the left-hand side of Eq. (9) is the viscous damping of the membrane due to the surrounding fluid, and the second term is the restoring force due to the curvature stiffness of the bilayer. Here, $\eta \sim 3\eta_{water}$ is a slightly enhanced, effective viscosity due to the cytoskeleton confinement of the membrane fluctuations [12,28].

At the scale of a single spectrin network unit cell, the membrane has a characteristic fluctuation frequency: $\omega_m \simeq \kappa/4\eta a^3 \sim 10^3$ Hz. This should also include the re-association time τ_{re}, which is the Zimm time it takes the detached end of the filament to thermally diffuse back to the attachment site and re-attach [33]. Since the detached spectrin is confined by the bilayer, only a short segment of the spectrin molecule can actually diffuse freely. This results in $\tau_{re} \sim 10^{-7}$ s, which can therefore be neglected.

For the RBC case, where $\omega_m \leqslant \tau^{-1}$ (in normal conditions), we can write [18]

$$\langle |h|^2 \rangle_{ATP} \simeq a^2 \frac{\Delta E}{\kappa} \frac{\mu a^2}{\kappa} \frac{n_d}{1 + (\tau\omega_m)^{-1}} \sim \frac{a^2}{6} n_d \,, \tag{10}$$

where ΔE is the spectrin stretching energy defined above. The maximal r.m.s. height fluctuation due to ATP is $\langle |h|^2 \rangle_{ATP}^{1/2} \sim a/\sqrt{6} \sim 40$ nm. Note that the ATP-induced amplitude is proportional to the ratio of the tension released in the cytoskeleton and the curvature modulus of the membrane. This means that the motion on the length scale of the cytoskeleton network (~ 200 nm) is not thermal and does not satisfy the fluctuation-dissipation theorem [32,34].

The agreement [18] of our model for the effective temperature as a function of the ATP concentration with the data is rather good, except for low ATP concentrations, where there seems to be a threshold behavior in the experiments. This could arise from competing ATP-adsorption sites other than the spectrin–actin nodes, that effectively lower the available ATP concentration.

In addition to enhancing the membrane fluctuations, ATP-induced transient defects of the spectrin network are also important in determining the average shape of RBC [22,23]. ATP is clearly important for maintaining the discocyte shape of a free RBC, since it has been observed that depletion of ATP causes a change from the discocyte to the echinocyte shape [24]. This change of shape suggests that the loss of ATP results in a stiffer cytoskeleton that pulls the bilayer over a smaller cytoskeleton projected area. The need to accommodate the bilayer area over a smaller projected area results in the appearance of spicules of the echinocyte shape. In our model, the physical origin of this effect is simply related to the change in the number of released spectrin filaments, when the number of defects is reduced as ATP is reduced. We can estimate [18] this effect by estimating the resulting area difference between the interior and exterior membrane layers that has been suggested to drive the various shape transitions of RBC [24]. We relate this area difference to the pulling force that

the cytoskeleton exerts on the bilayer, and predict its dependence on the ATP concentration.

3. Cytoskeletal elasticity and cell shape

In the previous section we saw how the cytoskeleton provides a tension and a harmonic restoring force that affect the shape fluctuations of RBC. Defects in the cytoskeleton due to ATP activity may increase the fluctuation amplitude as well as induce shape changes. More dramatic effects [10] related to the reduction of the cytoskeletal elastic modulus have been observed in fibroblast cells and have been interpreted theoretically. In these systems, the cytoskeleton is a three-dimensional actin network whose elasticity is weakened by a drug that depolymerizes the actin polymers. On the molecular scale, there are many active, non-equilibrium processes that take place in the cell. However, on the scale of the slow time changes associated with changes in cell shape (several minutes), the microscopic events can be averaged to give effective elastic constants and surface tensions whose energetic balance determines the shape of nearly stationary cells.

The importance of actin in the majority of processes of cell morphogenesis allows one to probe in detail the changes arising upon gradual disruption of the actin cytoskeleton, using the drug Latrunculin A (LatA). LatA is known to bind monomeric actin by sequestering it. One thus controls the level of polymerized actin by varying the drug concentration [35]. A gradual [10] increase in LatA concentration leads first to arborization, the formation of numerous radial tubular protrusions, a phenomenon that has previously been described for other drugs that actively disrupt the actin cytoskeleton (Fig. 2). Further increase of the LatA concentration induces an instability of these tubes, converting them into a chain of pearls. This ''pearling'' is a general characteristic of fluid tubes under tension, that can be found in a wide variety of physical systems [36] including phospholipid bilayers [37]. The theory [10] accounts in a unified manner for both the shape changes and pearling instability as a function of the drug concentration.

3.1. Experimental observations

SVT2 cells [38] were plated on coverslips and treated with increasing concentration of LatA, $0.08\,\mu M \leqslant \Phi \leqslant 40\,\mu M$. Untreated cells are polygonal, with lamellipodia and protrusions concentrated in one or a few locations on the cell periphery as seen in Fig. 2. Their edges are curved, and the protrusions are at the vertices. This morphology is disrupted by the addition of LatA in two sequential stages. First, the outer envelope shrinks to form a round cell body enclosing the nucleus and most of the cytoplasm, leaving radial tubular processes still attached to adhesion points (''sun'' with ''ray'') as shown in Fig. 2. In the second stage, some of the tubes become unstable to the ''pearled'' state characteristic of tense cylinders. Complete recovery of cell shape occurs upon removal of LatA [10]. The dimensionless pearling wavelength, $\lambda_p = 2\pi R_0/k_p$, where R_0 is the unperturbed tube radius, also shows a

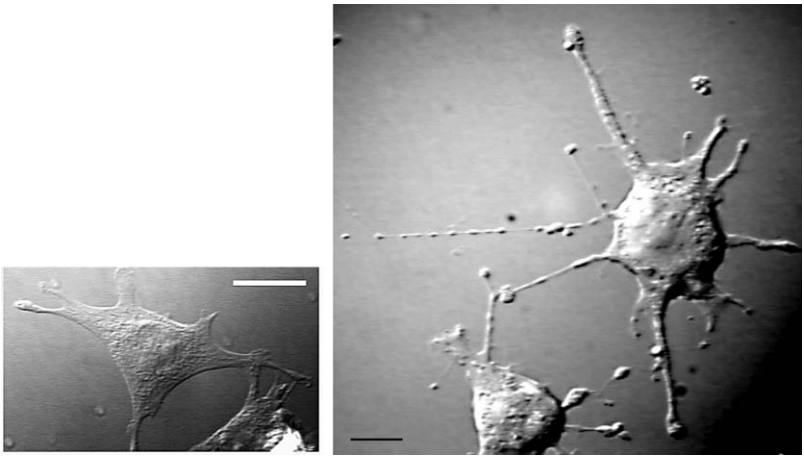

Fig. 2. The figure on the left shows an intact cell attached to a surface at several points (scale bar on the left figure is 20 μm). Note the semi-circular shape in between the attachment points. Arborization and pearling in an SVT2 cells treated with 2.5 μM LatA and fixed in paraformaldehyde are shown. The scale bar on the right figure is 10 μm (from Ref. [10], Copyright (1999), National Academy of Science, USA).

clear trend with Φ. Varying Φ by over two decades in the micromolar range, we obtained a clear power law behavior $k_p = (0.42 \pm 0.3)\Phi^{0.51\pm0.4}$ (with Φ in units of micromoles of LatA) over most of the range covered.

3.2. Theory

A simplified model for the cell shape as a function of the cytoskeletal elastic modulus regards the cell as an envelope that is attached to the substrate at several discrete locations. For relatively small concentrations of the drug, we assume that the cytoskeletal shear modulus, E, decreases linearly with the drug concentration Φ: $E = E_0 - \alpha\Phi$, where E_0 is the modulus of the drug-free cytoskeleton. The balance of forces in the cell will then depend drastically on the geometry. In its initial natural state, the adhering cell has a flattened shape, which is a stable configuration. Most of the elastic energy is located around the edge, due to the deformation of the actin cytoskeleton in that region. This gives an additional contribution to the effective line tension γ. Approximating the cross-section of the elastic edge as πh^2 gives $\gamma \simeq \pi E h^2$, where h is the average cell thickness near the edge.

One can minimize the total energy $\gamma \int \mathrm{d}l + \sigma \int \mathrm{d}S$ (elastic line tension of the edge and the surface tension energy of the entire cell, with the constraint that there are at least three attachment points) to obtain the force-balance equation $\sigma = \gamma/R_*$. Volume constraints are included by adjustment of the cell's vertical height, h. The equilibrium shape describes a positive curvature circular arc between the adhesion points, with radius $R_* = \gamma/\sigma \sim \pi E h^2/\sigma$. Approximating for the untreated cell $R_*(\Phi = 0) = 10\,\mu\mathrm{m}$ and $h \sim 1\,\mu\mathrm{m}$, while taking for the tension values typically

measured in cells $\sigma = 4 \times 10^{-2}\,\mathrm{erg/cm^2}$ [10], we obtain an estimate of $E_0 \sim 100\,\mathrm{Pa}$, consistent with Ref. [39].

As seen in both experiment and calculation, $R_* \sim E_0 - \alpha\Phi$ indeed decreases with Φ. At high values of the drug concentration, Φ, R_* decreases to a value smaller than the typical distance between adhesion points. In this case, most of the cell volume retracts into a nearly circularly symmetric region in the center connected to the adhesion points by thin tubes (see Fig. 2). The shape of the membrane near the cell center can be shown analytically to be close to a semi-circle, i.e., the distance between rays at the contact to the cell center is $L \approx 2R_*$. This prediction is well borne out experimentally ($L/R_* = 2$ within 10% on average).

At higher concentrations, the low surface to volume ratio favors a change of sign in the curvature of the outer envelope, the arborization process is complete and we obtain a "sun" as seen in Fig. 2. This shape has a circular (minimal surface) core containing the nucleus along with most of the cell cytoplasm, and rays attached to the original adhesion points.

We next estimate the effect of the elastic modulus on the pearling instability of the tubular protrusions. It is well known [36] that a fluid cylinder is unstable to formation of a string of spherical pearls due to their lowered surface energy [1]. This theory can be generalized to include the additional restoring force due a weak gel in the interior of the tube; the shear modulus of the gel suppresses the Rayleigh instability. Using a linear approximation, we consider the stability of a tube with an initial (undeformed) radius r_0, subject to a peristaltic perturbation of its radius, $r(z)$, of the form $r(z) = r_0 + u\sin(qz) - u^2/(4r_0)$, where r_0 is the tube radius, q is the wavenumber of the modulation and $u \ll r_0$ is its amplitude. The dimensionless wavevector is $k = qr_0$. Volume conservation is ensured by the term $u^2/4r_0$. The area of the tube, S, is reduced by a factor of $\delta S/S = (u/(4r_0))^2(k^2 - 1)$ and so the surface energy gain, per unit area, is $U_\sigma = \sigma(\delta S/S)$. A fluid cylinder under surface tension σ is thus unstable to long-wavelength modes with $k \leqslant 1$ [36], and the elastic forces oppose this instability.

For a gel-filled rod ($h = r_0$), the total elastic energy per unit area $U_T = \tilde{E}(4u/r_0)^2$ plus higher order terms of order k^2 and k^4, where $\tilde{E} = 3Er_0/(1+\sigma)$ is an effective cylindrical stretching modulus [10]. For all relevant wavelengths ($k \leqslant 1$), the k-dependent terms may be neglected for systems like cells where the shear modulus is weak. The new dimensionless criterion for stability is $-U_T/U_\sigma(q=0) = \tilde{E}/\sigma \geqslant 1$, which depends on the tube radius, r_0. It is therefore easier to destabilize thin tubes, requiring less drug and less disruption of the actin cytoskeleton. Since tubes are typically unstable when $r_0 \leqslant 1$–$2\,\mu\mathrm{m}$, and using $r_0 \sim h$, we get an estimate for the thickness of the actin cortex $h \leqslant 1\,\mu\mathrm{m}$. This also gives an estimate for the average Young's modulus at which pearling occurs, $E_p = (1+\nu)\sigma/(3r_0) \sim 20\,\mathrm{Pa}$. This rigidity is significantly lower than that of an untreated cell. The threshold for pearling occurs when the rigidity falls below a critical value corresponding to a critical concentration, Φ_c, typically of order $3\,\mu\mathrm{M}$.

Within a linear theory, we can find the growth rate of the instability by considering a small harmonic perturbation to a gel-filled rod $u(z,t) = u\mathrm{e}^{\omega t}\sin(qz)$. The time rate of change of the surface and elastic energies per unit length

is $\dot{U} = \pi\omega(u^2/r_0)(\sigma(k^2-1)+\tilde{E})$. The first term represents the tension energy while the second term is the positive shear rigidity contribution which tends to stabilize the tube. The growth rate of the instability is determined by equating $\dot{U}$ with the viscous dissipation of the Poiseuille flow of water in the deforming tube, $W = \eta(16\pi^3/5)\,\omega^2 k^{-2} u^2$, where η is the cytoplasm viscosity. The resulting dispersion relation takes the form

$$\omega(k) = \frac{5}{16\pi^2}\frac{k^2}{\eta r_0}\left(\sigma(k^2-1)+\tilde{E}\right). \tag{11}$$

The typical wavenumber of pearling at criticality is given by $k_c^2 = (\sigma - \tilde{E})/\sigma = (\Phi - \Phi_c)/(\Phi_0 - \Phi_c)$, where Φ_0 is the drug concentration at which the elastic modulus, $\tilde{E}$, vanishes. The theory predicts not only the observed square root dependence, but also the measured prefactor that gives an estimate for Φ_0 on the order of 10 μM. This simple theory seems to reasonably estimate the value at which the actin has lost almost all efficacy. However, the simple linear dispersion relation cannot predict the full nonlinear dynamic relation relevant at late times.

4. Cytoskeletal elasticity and cell adhesion

Adhesion of live cells to external surfaces [40] plays an important role in many cellular processes, such as cell growth, differentiation, motility and apoptosis (programmed cell death) [41]. Cell adhesion is not a passive process, restricted to the formation of bonds between membrane receptors and extracellular ligands. Adhering cells actively probe the physical properties of the extracellular matrix; their cellular contractile machinery participates in the formation of the adhesive junctions in a manner that is not yet understood. It has been shown that on rigid surfaces, the interaction of the contractile machinery of the cell and adhesions gives rise to large and stable junctions, termed focal adhesions (FA). These are associated with the termini of actin stress fibers and trigger signaling activity that affects gene expression, cell proliferation and cell survival. On the other hand, soft surfaces mainly support the development of relatively small, transient, dot-like or fibrillar adhesions that are involved respectively in cell motility and matrix reorganization. In addition, observation of the early phase in the assembly of FA shows small, primordial adhesions, termed focal complexes (FX) as precursors of FA. FX are formed close to the edge of the advancing membrane protrusions of cells and can sometimes develop into FA when subjected to mechanical stress due to either cell contractility or external perturbations [42]. Indeed, the adhesion process has been shown to be mechanosensitive; cells can probe the physical properties of their environment and respond by modulating the biochemistry of their adhesions or migratory activity [7,43,44].

Live cells exert directional, lateral forces on adhesive junctions; these forces originate from the interaction of the contractile cytoskeleton (actin filaments and their associated myosin motors) and the adhesion sites (Fig. 3). Adhesions respond dynamically to the local stresses: increased contractility leads locally to larger

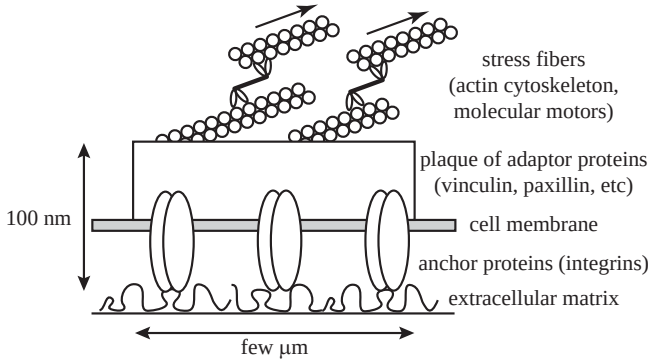

Fig. 3. Schematic representation of an FA (from Ref. [71], Copyright (2004), National Academy of Sciences, USA).

adhesions [5], whereas FA are disrupted when myosin II is inhibited [45]. Conversely, growth of FA is observed when force is applied externally, e.g., by a micropipette, rather than internally by actomyosin contractility. The physics challenge in the understanding of these effects lies in (i) quantifying on a coarse-grained scale the forces that cells exert on surfaces or in the bulk, (ii) understanding the implication of these forces for adhesion of a single cell, the interactions among many cells in an elastic medium and the consequent self-assembled structures that may form and (iii) predicting the microscopic origin of these forces and why adhesion growth is sensitive to the magnitude and direction of the internal or external cytoskeletal stresses.

4.1. Lateral forces at adhesion sites

Biological cells can exert strong physical forces on their surroundings. One example are fibroblasts, that are mechanically active cells found in connective tissue. In the early 1980s, Harris and coworkers [46] found that fibroblasts exert surprisingly large forces on surfaces. They suggested that strong fibroblast traction is needed in order to align the collagen fibers in the connective tissue. Since cell locomotion is guided by collagen fibers, this results in a *mechanical interaction* of cells. The interplay of fiber alignment and cell locomotion has been analyzed theoretically in the framework of coupled transport equations for fiber and cell degrees of freedom [47]. However, it is well known that cellular behavior is also affected by purely elastic effects, which were not considered in these studies. For example, stationary cells plated on an elastic substrate that is cyclically stretched reorientate away from the stretching direction [8], and locomoting cells on a strained elastic substrate reorient in the strain direction [44]. Recent experiments also show that adhering cells sense mechanical signals through FA [5,45]. In contrast to chemical diffusion fields, elastic effects are long-ranged and propagate quickly. They are known to be important during development, wound healing, inflammation and metastasis [48].

The main technique used to measure cellular forces is the elastic substrate method [49] which was introduced by Harris and coworkers in the early 1980s [46]. A thin elastic film over a fluid is produced; under cell traction the film shows a wrinkled pattern, which is characteristic of the pattern of forces exerted. However, deformation data can be analyzed only semi-quantitatively with this technique, because the buckling of thin polymer films is a nonlinear phenomenon that is very difficult to treat in elasticity theory. Quantitative analysis of elastic substrate data was pioneered by Dembo and coworkers. Using linear elasticity theory for thin elastic films and numerical algorithms for solving inverse problems, the surface forces exerted by keratocytes could be reconstructed [50]. One key ingredient of this method is the use of a regularization scheme, because the inverse problem is ill-posed and is thus highly sensitive to noise in the data for the displacement.

Recently, a novel elastic substrate technique to measure cellular forces at the level of single FA [5] was developed. A thick polymer film made from PDMS with a Young's modulus $E \sim 10$–$20\,\mathrm{kPa}$ and Poisson ratio $v \sim 0.5$ was micropatterned by standard lithographic techniques. Cell traction was generated by stationary, yet mechanically active cells (human foreskin fibroblasts, cardiac fibroblasts or cardiac myocytes). The cells are treated to express green fluorescent protein (GFP)-vinculin that is a protein found in FA and thus indicates the size and shape of the adhesion. Since traction was never observed near an area deprived of FA, it was assumed that FA are the main sites of application of force by the cells. This permitted the development of a numerical procedure to reconstruct discrete forces at the sites of the FA. Correlation with the lateral size of the FA showed that there exists a linear relationship between force F and area A of a single FA. This finding translates into a force of few pN per receptor, which is consistent with recent measurements of the strength of single molecular bonds at slow loading [51].

Since the adhering cells are rather flat, the tension forces exerted on the substrate can be considered to be tangential to the plane of the substrate surface. Also, because surface displacements are much smaller than film thickness, one can use linear elasticity theory for an elastic isotropic half-space. For incompressible elastic substrates ($v \sim 0.5$), the resulting displacement of the substrate surface remains within the plane of the substrate surface [52]. Therefore, the entire elastic problem becomes two-dimensional. Consistent with the observations, it is assumed that forces are exerted mainly at the sites of FA. For a single, discrete force density (force per unit volume) $\vec{f}$ at position $\vec{r}$, the displacement field $\vec{u}$ at position $\vec{r}$ is

$$u_i(\vec{r}) = \int \mathrm{d}\vec{r}'\, G_{ij}(\vec{r} - \vec{r}') f_j(\vec{r}')\,, \tag{12}$$

where the subscripts refer to the vector components (summation over repeated indices is implied) and where G_{ij} is the Green function of the elastic isotropic halfspace—a tensor of rank two:

$$G_{ij}(\vec{r}) = \frac{3}{4\pi E r}\left(\delta_{ij} + \frac{r_i r_j}{r^2}\right). \tag{13}$$

Note that in finite systems, $G_{ij}(\vec{r}-\vec{r}')$ is an explicit function of both $\vec{r}$ and $\vec{r}'$. This is because the elastic forces can be long range and thus depend on the boundary conditions. In the case of the half-space, the displacements are mostly in the plane; there are negligible normal displacements and the translational symmetry is approximately restored. Here, δ_{ij} denotes Kronecker delta and E Young's modulus. The Poisson ratio has been set to $\frac{1}{2}$, the value for incompressible systems. The indices i,j take the values $1,2$ corresponding to the x and y directions. One generalizes the above to treat a set of discrete forces exerted at the sites of the observed FA. One must solve the inverse problem of predicting the forces, given the observed displacement and the resulting force pattern turns out to be very sensitive to small changes in the displacement data. To regularize the problem [53], we use the reasonable constraint that the forces should not be exceedingly large.

This approach allowed the measurement of cellular forces at the level of FA and its correlation with aggregation characteristics of the proteins that comprise the FA [5]. Fig. 4 shows a computer representation of the different data sets used in the analysis. The square arrangement of the small arrow represents the deformation field from image processing of the phase contrast pictures of the micropatterned substrate. The ellipses represent fits to the FA found from image processing of the GFP-vinculin fluorescence images. The large arrows at the midpoints of the FA represent the forces calculated from the data for the deformation and the location of

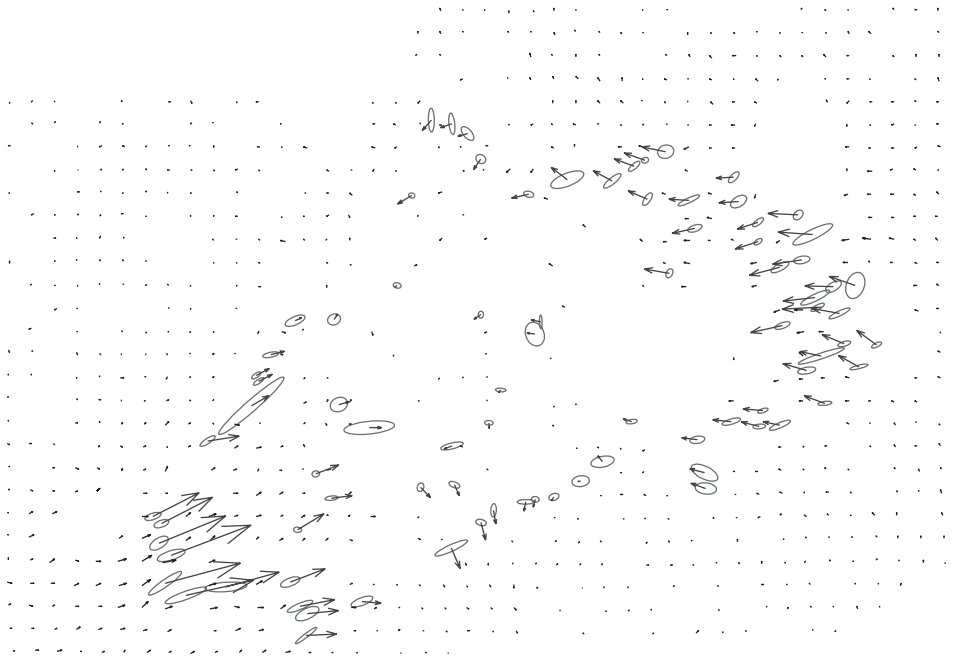

Fig. 4. Forces exerted by fibroblast cells [5] on patterned substrates. The forces are deduced from the measured deformations of the substrate as described in the text. The arrows indicate the forces exerted by the FA that are shown as elliptical regions.

the FA. Typical forces at mature FA of human foreskin and cardiac fibroblasts were found to vary between 10 and 30 nN. Since each cell can have several hundred FA, the overall force exerted by a single cell goes up to the μN range. The main result was that force correlates strongly with aggregation of the proteins that comprise the FA. One finds a linear relationship between magnitude of force and FA area. The direction of force usually agreed with FA elongation. For larger areas, force grows in proportion with area, with a stress constant of $5.5\,\mathrm{nN}/\mu\mathrm{m}^2$.

The relation between force and size of the FA indicates that they act as mechanosensors: forces are used to actively probe the mechanical properties of the environment [48]. In particular, it has been shown that forces applied at FA are converted into biochemical signals that trigger signalling pathways (see below), related to the aggregation behavior of the proteins that comprise the FA.

4.2. Elastic interactions of cells: force dipoles

Anchorage-dependent cells constantly assemble and disassemble FA, thereby probing the mechanical properties of their environment. Initial protein aggregates (FX) are the precursors of FA. If the initial clustering is further stabilized by the properties of the extracellular environment, FX can mature into FA. In this case, they connect to the actin cytoskeleton and a contractile force pattern builds up, that is actively generated by myosin II molecular motors interacting with the actin cytoskeleton. The minimal configuration of this machinery is a set of two FA connected by one bundle of actin filaments (*stress fiber*), that leads to a pinch-like force pattern. In condensed matter physics, such an object is known as an *anisotropic force contraction dipole* [54]. The concept of force dipoles has been applied before mainly for the description of defects and intercalants in "hard" condensed matter systems [55–57]. The concept of force dipoles has also been used to model active biological particles in a fluid environment [58–60].

By analogy with electric dipoles, a force dipole, P_{ij}, is a second rank tensor defined as the second moment of a spatially distributed force density (force per unit volume), $\vec{f}(\vec{r})$,

$$P_{ij} = \int \mathrm{d}\vec{s}\, s_i f_j(\vec{s})\,, \tag{14}$$

where the subscripts refer to the vector components. The elastic deformation field $\vec{u}(\vec{r})$ is related to the force distribution and to the Green function as given in Eqs. (12) and (13). If the force distributions are described in terms of force dipoles, the displacement field at point $\vec{r}$ due to a dipole at point $\vec{r}'$ can be written [7] as

$$u_i(\vec{r}) = G_{il,k'}(\vec{r},\vec{r}')P'_{kl}\,, \tag{15}$$

where the extra index denotes a derivative of the Green function with respect to the variable $\vec{r}$; a prime on this index indicates that the derivative is with respect to the variable $\vec{r}'$. As before, there is an implied summation over repeated indices. The prime on P indicates that the dipole is located at position $\vec{r}'$. The interaction of two

dipoles proceeds via the deformation of the medium; each dipole feels the deformations induced by the other and this creates an effective interaction between them. For dipoles that are located at $\vec{r}$ and $\vec{r}'$, one can derive the effective interaction due to the elastic deformation energy of the medium. One finds that the elastic deformation of the medium contributes to the effective interaction given by the product of the force dipole and the strain (i.e., the derivative of the displacement $\vec{u}$) [7]. This energy, $W>0$, has a contribution from the deformation of the medium by each dipole and an interaction term, W', which is:

$$W' = P_{li}u_{i,l} = P_{li}G_{ij,lk'}(\vec{r},\vec{r}')P'_{kj}\,, \tag{16}$$

where P_{li} and P'_{kj} are the force dipoles located at $\vec{r}$ and $\vec{r}'$ respectively, $u_{i,l}$ is the derivative of the displacement component u_i with respect to component l of the position vector $\vec{r}$ and the last two subscripts in the Green function represent derivatives with respect to $\vec{r}$ and $\vec{r}'$ respectively. For translationally invariant systems, such as an elastic half-space with planar displacements,

$$G_{ij,lk'}(\vec{r},\vec{r}') = G_{ij,lk'}(\vec{r}-\vec{r}') = -G_{ij,lk}(\vec{r}-\vec{r}')\,. \tag{17}$$

This interaction energy scales as $1/|\vec{R}|^3$ where $\vec{R}$ is the distance between dipoles and is proportional to P^2/E, where P is the dipole strength and E is the Young's modulus of the medium. Eq. (16) is not the only relevant energy to be considered since in the case of inert matter one must add to the deformation energy of the medium an energy proportional to the product of the local force and the local displacement; this is the direct interaction of the dipole with the environment which is the driving force for self-assembly, since the elastic energy arising from the deformation of the medium (W from Eq. (16)) is always positive. The elastic theory can also describe the interaction of a single dipole with an external strain imposed on the elastic medium [7].

Recently, we have extended the concept of force dipoles to model the mechanical activity of cells [6]. Cells in an isotropic environment often show isotropic (that is round or stellate) morphologies. However, since the FA dynamics is local, even in this case there is an anisotropic probing process, that can be modeled by anisotropic force *contraction* dipoles. The anisotropy of FA dynamics becomes apparent when stress fibers begin to orient in one preferential direction, either spontaneously during a period of large mechanical activity, or in response to some external anisotropy, or during cell locomotion. In this case, cellular dipoles have been measured to be of the order of $P \approx -10^{-11}$ J (this corresponds to two forces of 200 nN each, separated by a distance of 60 μm) [5,61]. In Fig. 5, we show schematic representations of the physical and cellular cases discussed here.

In order to sense the mechanical properties of their environment, cells can make use of the fact that these properties modulate the build-up of their own force patterns. In order to calculate how stress and strain are propagated in the environment, the extracellular material is modeled using isotropic linear elasticity. Given this assumption, one can calculate how the stress and strain related to the force dipoles by solving the elastic equations for the geometry and boundary conditions of interest [6,7]. In terms of the displacement field, $\vec{u}(\vec{r})$, this amounts to

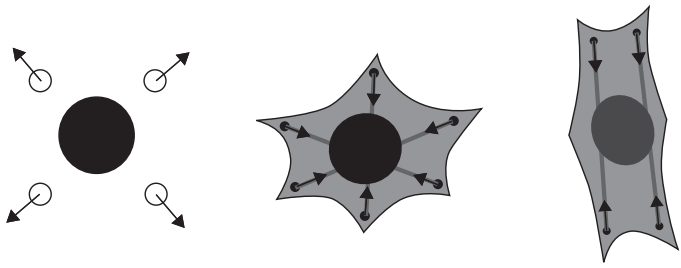

Fig. 5. Schematic representation of physical and cellular force dipoles. (a) Physical case: an intercalated defect deforms the simple cubic host lattice, thus acting as an isotropic force expansion dipole. (b) Cellular case: anchorage-dependent cells probe the mechanical properties of the soft environment through their contractile machinery. Actin stress fibers (lines) are contracted by myosin II molecular motors and are connected to the environment through FA (dots). Even if cell morphology is round or stellate, different stress fibers probe different directions of space and compete with each other for stabilization of the corresponding FA. Therefore, the probing process can be modeled as an anisotropic force contraction dipole. (c) Cell morphology becomes elongated in response to anisotropic external stimuli, during locomotion or spontaneously during times of strong mechanical activity. Then most stress fibers run in parallel and the whole cell acts as an anisotropic force contraction dipole. (Reprinted with permission from Bischofs and coworkers [7], Copyright (2004) by the American Physical Society.)

solving the linear second-order differential equation

$$\Delta\vec{u}(\vec{r}) + (1+\Lambda)\nabla\nabla\cdot\vec{u}(\vec{r}) = -\frac{\vec{f}(\vec{r})}{\mu}, \quad \vec{r} \text{ in } V, \tag{18}$$

where the body forces, $\vec{f}$, on the right-hand side are determined by the distribution force dipoles and where $\Lambda = \lambda/\mu$ is the ratio of the Lamé coefficients [7]. Note that this equation is difficult to solve because the second term on the left-hand side couples the different components of the displacement vector.

The most critical part of the model is the way in which physical or cellular force dipoles react to stress and strain in their environment. This subject has been treated extensively for the case of atomic defects in traditional condensed matter systems [55–57]. Here defects are usually modeled as isotropic force *expansion dipoles*. The equilibrium configuration follows by minimizing the sum of the elastic energy of the strained medium and the direct interaction energy between force dipole and elastic environment. The first term represents a restoring force and raises the energy (i.e., its sign is always positive), while the second term is a driving force that reduces the total energy (i.e., its contribution will always be negative). The total interaction between two dipoles has the form of Eq. (16) but with a negative sign due to the effect of the local force–displacement interaction.

The equilibrium configuration will correspond to the minimum of the total energy as a function of position and orientation of the force dipoles, which results in an effective, so-called *elastic interaction* between the force dipole and other dipoles, sample boundaries or external strain fields. One central result of these studies is that

the direct interaction between isotropic force dipoles in an isotropic elastic material vanishes [54] and that they interact through a boundary-induced (*image*) interaction that varies on the length scale of the sample size (leading to *macroscopic modes*) [55]. For anisotropic force dipoles, the direct elastic interaction does not vanish. Recently, we have predicted that the competition between direct and image interactions should lead to hierarchical structure formation, with the direct interaction leading to structure formation on a length scale set by the elastic constants and similar to that of electric quadrupoles [6]. We suggested that such a behavior should be expected for artificial or inert cells, that is for physical particles with a static force contraction dipole, but without any internal dynamic or regulatory response.

In contrast to this physical case, the effective behavior of active cells usually follows from dynamic and highly regulated non-equilibrium processes inside the cell. More recently, we have shown that despite this severe complication, it is still possible to describe the active response of mechanosensing cells in an elastic material in the same framework as the physical case [7]. Motivated mainly by recent experiments with elastic substrates [43,44,62], we have suggested that effective cellular behavior can be described as simple preference for large effective stiffness in the environment (including both rigidity and tensile prestrain). Moreover, one can show that this principle is equivalent to minimization of the energy which the cells have to invest in straining the environment in order to build-up the force dipole used for probing the mechanical properties of the environment, but not the energy due to the direct force–displacement interaction. This results in an interaction energy between two force dipoles with a positive sign as given in Eq. (16).

One likely explanation for the observed active behavior of cells is that the build-up of force at FA is more efficient in a stiff environment. Since this approach allows one to use the same framework as in the physical case, we were able to derive elastic interaction laws between cells and their elastic environment which are in good agreement with experimental observations for fibroblasts both on elastic substrates and in hydrogels. In particular, the direct elastic interaction between cells has been predicted to be similar to that of electric dipoles, leading to strings of cells [7]. This is not the case for inert dipoles (due to the difference in the sign of their interaction) where more compact structures are predicted [6,7].

Bischofs and coworkers [7] considered in detail the interactions of cells with external strain fields, sample boundaries or other physical force dipoles/cells. Although there are marked conceptual differences between the physical and cellular cases, they both involve the elastic boundary value problem to predict the resulting structure formation. Since cells are modeled as anisotropic force dipoles, these calculations are in general more involved than similar calculations for isotropic force dipoles. Moreover, in contrast to earlier calculations for the physical case, one is interested not only in the effect of free but also of clamped boundaries, which are known to induce mechanical activity of cells [63].

For example, consider a cell inside an elastic half-space. This cell is characterized by a distance d to the surface, an angle θ with respect to the surface normal and a

force dipole moment P. Exactly solving the corresponding elastic equations leads to

$$W = \frac{P^2}{256\pi E d^3}\,(a_v + b_v \cos^2\theta + c_v \cos^4\theta)\,, \tag{19}$$

where E is the Young's modulus and where the coefficients a_v, b_v and c_v are complicated functions of the Poisson ratio v calculated for both free and clamped boundary conditions in Ref. [7]. The result scales quadratically with P because the cell effectively interacts with its boundary-induced image. Minimizing the interaction energy, W, predicts that cells orient parallel and perpendicular to free and clamped boundaries, respectively, as has been observed before in many experiments. Although this result is somehow intuitive [cells prefer (avoid) clamped (free) boundaries because they effectively increase (decrease) the stiffness of the environment], it is important to note that our calculations not only predict the most favorable organization, but also the elastic differences cells sense when probing different positions and orientations.

The different energies and opposite sign of the interactions for the case of inert force dipoles and active cell force dipoles lead to interesting differences in their behavior. For example, active cells are attracted and repelled by clamped and free sample boundaries, respectively. In the case of inert dipoles, this behavior is inverted. The predictions for the elastic response cells explain several experimental findings reported in the literature [7] and can be used for rational design of tissue equivalents. Again, it is important to note that the application of soft matter physics principles to biological matter requires consideration of the active processes. In the case of cell elastic interactions, this means that only the deformation energy of the medium is important in determining the effective cell–cell interaction. This is in contrast to the case of inert dipoles where the total energy must be considered.

5. Theoretical model for mechanosensitivity of adhesion

5.1. Cell adhesion mechanosensitivity

The experiments described above indicate that adhering cells exert lateral forces on adhesion sites due to the internal tension of the cytoskeletal stress fibers. The size and anisotropy of the adhesion sites are correlated with these forces and this makes adhering cells quite different from adhering vesicles which have no internal stresses. The coupling of the internal stresses which can be regulated by the cell (e.g., via actin–myosin activity or actin polymerization) means that the cell can respond to the elasticity of its adhesive environment. As we saw previously, this regulates not only the local adhesion of a given cell, but also the interactions of many cells and their subsequent self-assembly into larger scale structures. Recent experiments have shown that external forces can also cause the anisotropic growth of FA. Independent of the origin of the stress (e.g., internal contractility [5], shear flow [64], micropipette-induced shear stress [45]), small adhesions grow into FA, that elongate in the direction of the force. The FA grows via a biochemical process that is very sensitive

to the force applied to the adhesion region by the cytoskeleton, and the origin of this mechanosensitivity is an important problem in cell biology since adhesion influences cell viability.

Our model (see Fig. 3) assumes that the biochemical response of adhesions to cytoskeletal stresses originates from the stress-induced elastic deformation of the adhesion site. These force-induced deformations modify the local density of the proteins found in and around the adhesive junction, and thus their interactions. We suggest that this, in turn, can trigger a conformational change or a molecular reorganization that initiates the biochemical cascade responsible for the aggregation of new proteins and the directional, anisotropic growth of the adhesion. As a specific example, transmembrane, integrin proteins could be the mechanosensor [42], since they are connected to the extracellular matrix and are elastically deformed by cytoskeletal forces; this deformation can activate conformational or organizational changes which enhance their binding with plaque proteins [41].

In addition to the fact that adhesion to an anchoring surface makes a junction sensitive to shear [65] (even if the latter is composed of fluid-like assemblies of molecules), several observations support the view we propose. First is the observation that independent of the origin of the stress, small adhesions grow into FA, that elongate in the direction of the force. This anisotropy is predicted by our theory since stress-induced deformations are correlated with the applied force and exert different effects on the proximal (front) and the distal (back) aspects of the adhesive junctions.[1] In our model, where we relate the biochemical response to deformations, this anisotropy also leads to an anisotropic addition (or loss) of proteins. Moreover, the size and the strength of the adhesive junctions depend on the elastic properties of the extracellular matrix [66,67]. Our model predicts that the extent and the nature of the adhesion is sensitive to the mechanical properties of the underlying matrix: a local force applied to an adhesive junction induces a pure translation of the junction (and thus no deformation) if the extracellular matrix is very soft, whereas strongly grafted adhesions on a rigid matrix are elastically deformed by local, lateral stresses.

5.2. *Description of the model*

The total force transmitted by FA has been shown to be proportional to their surface area [5], suggesting that the region over which stress fibers act grows with the junction. As a model, we consider the adhesion and its membrane-associated integrins as an elastic, thin film grafted at its bottom surface and stressed by a local lateral force on its top surface; ''local'' means here that the force only acts on a finite region of the adhesive junction, which, as explained below, needs only to be somewhat smaller than the total area of the adhesion by a few thicknesses of the FA (typically, a few tens of nanometers). One possible scenario is that the integrin layer

[1]The front and back edges of the adhesion are defined relative to the direction of the force induced by stress fibers. They should not be confused with the front and the back of a moving cell (see Fig. 3).

forms in advance of the adhesion protein plaque and the associated stress fibers, so that the stressed region is smaller than the adhering integrin cluster [68].

The localization of the force is a crucial aspect of our model, since a homogeneously applied stress would give rise to a uniform shear of the adhesive junction and a translational motion of the surrounding lipid membrane. Since the latter is not grafted to the surface, no anisotropic density changes in the protein layer can occur and no directional, force-induced biochemical response can arise from a homogeneous lateral stress. By contrast, a *local*, tangential stress induces a compression at the front edge and an expansion at the back of the stressed region because the unstressed part is also grafted and cannot slide. In this case, a lateral force induces anisotropic density changes in proteins located inside or close to the stressed region. The resulting, stress-induced deformation profile can be calculated using continuum elasticity theory [65]. Our model assumes that this change in density triggers the biochemical response responsible for the growth or dissolution of FA. Anisotropic variations of density thus give rise to different molecular dynamics in the front and back regions near the edge and can result in either overall growth or shrinking of the FA as shown below.

We first consider a quasi-two-dimensional model of FA in which the elastic thin film is represented by particles that interact via springs of stiffness k_0 (see Fig. 6). The particles are bound to the anchoring surface by springs of stiffness k_b, that measure the resistance to normal shear and are therefore related to the normal shear modulus. Each particle in our model is a protein complex consisting of one integrin molecule and the associated intracellular proteins that connect it to the actin cytoskeleton; this we define as the minimal complex of proteins needed for the adhesion to grow. The elastic properties of the extracellular matrix and its connection to the anchoring surface are included by fixing the anchors to the surface via a sinusoidal potential which, in the limit of small displacements, reduces to a spring-like interaction where k_m is the stiffness of the anchorage close to the equilibrium position. The case of a layer grafted onto a rigid and immobile extracellular matrix (discussed next) is found by taking the limit $k_m \to \infty$.

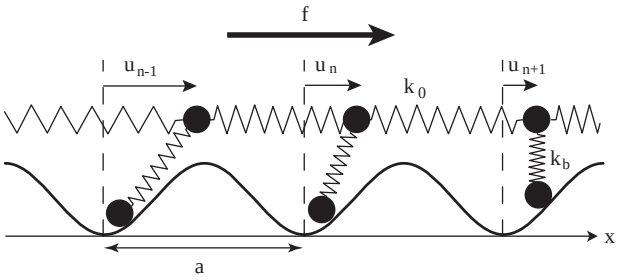

Fig. 6. One dimensional chain of interacting particles bound to anchors, as a model for FA grafted to an extracellular matrix. The potential $V(x)$ accounts for the grafting properties of the extracellular matrix. The distance a between the anchors is the integrin-integrin spacing and u_n is the displacement of the n^{th} particle from its position in absence of force. (From Ref. [71], Copyright (2004), National Academy of Sciences, USA.)

5.3. Predictions of the model

In a one-dimensional version of this approach (Fig. 6, which can easily be generalized to a two-dimensional layer), the mechanical equilibrium for such a system of particles pulled by a force $F(x)$ is, in the continuum limit,

$$k_0 a^2 \frac{d^2u}{dx^2} - k_b u + F(x) = 0\,, \tag{20}$$

where k_0 is the spring constant connecting the particles to each other and k_b accounts for the restoring force due to the connections to the fixed and rigid extracellular matrix. We solve Eq. (20) for a gate-shaped field of force of amplitude, f, per unit length and width L; that is, the force is only non-zero for $-L/2 < x < L/2$. This force profile corresponds to the *local* pulling force due to stress fibers, and induces the following spatial variation of the local, average density, $\delta\Phi(x)$, relative to the undeformed density Φ [65]:

$$\frac{\delta\Phi}{\Phi}(x) = -\frac{du}{dx} = \frac{f}{\sqrt{k_b k_0}} \begin{cases} \sinh \frac{x}{\ell}\, e^{-L/2\ell} & \text{if } |x| < L/2\,, \\ \sinh \frac{L}{2\ell}\, e^{-|x|/\ell}\ \mathrm{sign}(x) & \text{if } |x| \geqslant L/2\,. \end{cases} \tag{21}$$

Eq. (21) is derived for the case of a stiff matrix ($k_m \to \infty$) and shows that the deformation decreases exponentially with a range $\ell = a\sqrt{k_0/k_b}$. Remembering that an actual adhesion has a finite thickness fixes the order of magnitude of ℓ: force-induced deformations must vanish at the bottom surface due to the grafting boundary condition appropriate to the case of an immobilized extracellular matrix. Thus the range ℓ is of the order of the thickness of the junction ($\sim 100\,\mathrm{nm}$). The representation of the adhesion as an infinite elastic medium pulled by a force acting on a finite region of size L is therefore valid once the actual size of the adhesion is larger than $L + 2\ell$, where $\ell \sim 100\,\mathrm{nm} \ll L$.

The three-dimensional case is treated more rigorously in Ref. [65] using a full elastic treatment of a thin film subject to a surface force, F, on its top surface with zero displacement boundary conditions at the bottom surface where the film is grafted to the substrate. The density, $\delta\Phi$, at the top surface is anisotropic and varies as

$$\delta\Phi \sim \frac{F}{E}\left(\frac{h}{\ell}\right)^3 \frac{e^{-r/\ell}}{\sqrt{r/\ell}} \cos\phi\,, \tag{22}$$

where ϕ is the azimuthal angle, E is the Young's modulus of the film, h is the film thickness, r is the distance from the edge of the applied force and, as above, ℓ is related to the thickness and a function of the film elastic constants [65]. This predicts a highly anisotropic response to the force in two dimensions and is consistent with the observation that the FA grow only in the direction of the applied force. The variation of density due to a local stress is only significant close (within a distance ℓ) to the edges of the stressed area. The predicted anisotropy means that changes in density are therefore much smaller on the sides of the stressed area perpendicular to the force, in accord with observations [45].

Typical estimates of the theoretical parameters include the following: (i) An assumption that each particle in our model contains one integrin, so that a ranges from 20 nm (close packing) to 80 nm [69]. (ii) Stiffness, k_b, of each protein complex is calculated from the Young's modulus, E, of the assembly of proteins: $k_b = Ea^2/h$, where h is the vertical thickness of the adhesion and E is in the range 10^3–10^6 Pa [70]. The rigidity of a particle of area a^2 is therefore in the range 10^{-3}–10^2 mN/m. (iii) The force per unit length, f, on each particle is extracted from the measurement in Ref. [5]: $f = 5.5\,\mathrm{nN}/\mu\mathrm{m}^2 \times a$. The estimates imply that the variations of density induced by the stress dominate variations induced by thermal fluctuations by at least one order of magnitude.

5.4. Growth of FA

The main hypothesis of our model is that force-induced deformations trigger the biochemical response of FA, via conformational (e.g., activation of integrins) and/or organizational changes (e.g., binding of plaque proteins) of molecules embedded in a narrow region of size ℓ where the density varies. This local activation increases the rate of association of free proteins within this area. The competition of the elastic and biochemical energies determines whether additional proteins will join the FA. Within our model, the addition of a protein complex of size a to the FA results in a deformation with an elastic energy cost ΔE_{el} proportional to $f^2a^2/2k$ where $k = k_b k_m/(k_b + k_m)$ (where k_m is defined above) is an effective elastic constant that includes the finite stiffness of the extracellular matrix [71]. We now suppose that the association of a free protein complex to the front edge of the adhesion releases an energy ΔE_a that depends on the change in density at the front edge of the stressed region. In the absence of density variations, the probability of attaching a new particle is unchanged, and $\Delta E_a = 0$. For small variations of the density, ΔE_a can be taken to vary linearly with the change in density at the edge. This energy also scales with the free energy of reaction of one protein complex, e. Adding a protein complex to an adhesive junction thus involves an overall variation of free energy:

$$\Delta E = \frac{f^2a^2}{2k} - e\,\frac{f}{\sqrt{kk_0}}\,. \tag{23}$$

We first discuss the case where $e<0$: aggregation of new particles to an existing adhesion is thermodynamically unfavorable ($\Delta E>0$ always), and an additional input of energy is required to stabilize the protein cluster. Such input of energy may come from fluctuations arising from active processes in the surroundings, as opposed to thermal fluctuations which are small compared to the required energies. However, on the time scale of growth of an adhesion (10–20 min), only a limited amount of external energy is available and the adhesions can only grow to a finite size. For this thermodynamically unfavorable growth process, increasing the force f per unit length thus leads to smaller adhesions. This is in contrast to the observations [45], so we conclude that FA do not correspond to the case where $e<0$.

FA can only grow when the overall free energy of Eq. (23) is negative, corresponding to $e>0$—i.e., favorable aggregation energy and an exothermic, local chemical interaction. However immobilization of the extracellular matrix ($k_m \to 0$) or very large forces can lead to positive value for ΔE, and, if large enough, may arrest the growth process, even if $e>0$. This effect is indeed observed: large forces disrupt FA [72]. The analysis presented here can be generalized to predict the kinetics of growth of FA ahead of the pulling force applied by the cytoskeleton or an external force and the dissolution of FA in back of the force [71]. Alternative models of the kinetics of growth of FA that use a uniform model for the applied force have also been suggested [73]. Although the primary trends predicted for the anisotropic growth and its dependence on the substrate elasticity agree with the experimental observations, quantitative comparison of the model and both static and dynamic experiments will lead to further refinement and enhance our understanding of the physics of adhesion.

Acknowledgements

The authors acknowledge very fruitful experimental collaborations with L. Addadi, N. Balaban, R. Bar-Ziv, A. Bershadsky, A. Bitler, B. Geiger, R. Kornstein, E. Moses, D. Riveline, E. Sackmann and H. Strey and theoretical discussions with I. Bischofs, M. Kozlov and A. Zilman. This work has been supported by the Israel Science Foundation, the US–Israel Binational Science Foundation, the Minerva Foundation, the German–Israel Foundation and an EU Network Grant. U.S.S. has been supported by the Minerva Foundation and the German Science Foundation through the Emmy Noether Program.

References

[1] S.A. Safran, Statistical thermodynamics of Surfaces, Interfaces, and Membranes, Westview Press, Boulder, 2003.
[2] B. Alberts, D. Bray, J. Lewis, M. Raff, K. Roberts, J. Watson, Molecular Biology of the Cell, Garland Publishing, New York, 1994.
[3] D. Boal, Mechanics of the Cell, Cambridge University Press, Cambridge, 2002.
[4] B. Geiger, A.D. Bershadsky, Cell 110 (2002) 139.
[5] N.Q. Balaban, U.S. Schwarz, D. Riveline, P. Goichberg, G. Tzur, I. Sabanay, D. Mahalu, S.A. Safran, A.D. Bershadsky, L. Addadi, B. Geiger, Nat. Cell Biol. 3 (2001) 466.
[6] U.S. Schwarz, S.A. Safran, Phys. Rev. Lett. 88 (2002) 048102.
[7] I.B. Bischofs, U.S. Schwarz, Proc. Natl. Acad. Sci. USA 100 (2003) 9274;
I.B. Bischofs, S.A. Safran, U.S. Schwarz, Phys. Rev. E 69 (2004) 021911.
[8] P.C. Dartsch, H. Hämmerle, E. Betz, Acta Anat. 125 (1986) 108;
J.H.-C. Wang, E.S. Grood, Connect. Tissue Res. 41 (2000) 29.
[9] K. Jakab, A. Neagu, V. Mironov, R.R. Markwald, G. Forgacs, Proc. Natl. Acad. Sci. USA 101 (2004) 2804.
[10] R. Bar-Ziv, T. Tlusty, E. Moses, S.A. Safran, A. Bershadsky, Proc. Natl. Acad. Sci. USA 96 (1999) 10140–10145.
[11] V. Bennett, Bioch. Biophys. Acta 988 (1989) 107.

[12] N. Gov, A. Zilman, S. Safran, Phys. Rev. Lett. 90 (2003) 228101.
[13] N. Gov, S.A. Safran, Phys. Rev. E 69 (2004) 011101.
[14] E. Ling, Y.N. Danilov, C.M. Cohen, J. Biol. Chem. 263 (1988) 2209;
S. Manno, Y. Takakuwa, K. Nagao, N. Mohandas, J. Biol. Chem. 270 (1995) 5659.
[15] A. Zilker, H. Engelhardt, E. Sackmann, J. Phys. 48 (1987) 2139;
H. Strey, M. Peterson, E. Sackmann, Biophys. J. 69 (1995) 478.
[16] M.A. Peterson, Phys. Rev. A 45 (1992) 4116;
M. Peterson, H. Strey, E. Sackmann, J. Phys. II France 2 (1992) 1273.
[17] K. Zeman, H. Engelhard, E. Sackmann, Eur. Biophys. J. 18 (1990) 203.
[18] N. Gov, S.A. Safran, Biophys. J., in press.
[19] J.-B. Fournier, D. Lacoste, E. Raphael, Phys. Rev. Lett. 92 (2004) 018102.
[20] S. Tuvia, S. Levin, A. Bitler, R. Korenstein, J. Cell Biol. 141 (1998) 1551;
S. Levin, R. Korenstein, Biophys. J. 60 (1991) 733.
[21] E.A. Evans, Biophys. J. 43 (1983) 27;
M. Dao, C.T. Lim, S. Suresh, J. Mech. Phys. Solids 51 (2003) 2259.
[22] J.F. Hoffman, Blood Cell Mol. Dis. 32 (3) (2004) 335–340;
J.F. Hoffman, Blood Cell Mol. Dis. 27 (2001) 57.
[23] M. Nakao, Curr. Opin. Hematol. 9 (2002) 127.
[24] L.H.W. Gerald, M. Wortis, R. Mukhopadhyay, Proc. Natl. Acad. Sci. USA 99 (2002) 16766.
[25] D. Discher, N. Mohandas, E.A. Evans, Science 266 (1994) 1032;
H. Engelhardt, H. Gaub, E. Sackmann, Nature 307 (1984) 378.
[26] R. Everaers, I.S. Graham, M.J. Zuckermann, E. Sackmann, J. Chem. Phys. 104 (1996) 3774.
[27] A. Zilker, H. Engelhardt, E. Sackmann, J. Phys. 48 (1987) 2139.
[28] N. Gov, A. Zilman, S.A. Safran, Phys. Rev. E 70 (2004) 011104.
[29] F. Brochard, J.F. Lennon, J. Phys. 36 (1975) 1035.
[30] D.E. Discher, P. Carl, Cell. Mol. Biol. Lett. 6 (2001) 593.
[31] H.S. Seung, D.R. Nelson, Phys. Rev. A 38 (1988) 1005;
C. Carraro, D.R. Nelson, Phys. Rev. E 48 (1993) 3082;
J. Lidmar, L. Mirny, D.R. Nelson, Phys. Rev. E 68 (2003) 0519010.
[32] T.B. Liverpool, Phys. Rev. E 67 (2003) 031909.
[33] M. Doi, Introduction to Polymer Physics, Clarendon Press, Oxford, 1996.
[34] A. Bitler, R. Korenstein, submitted.
[35] M. Coue, S.L. Brenner, I. Spector, E.D. Korn, FEBS Lett. 213 (1987) 316;
K.R. Ayscough, J. Stryker, N. Pokala, M. Sanders, P. Crews, D.G. Drubin, J. Cell Biol. 137 (1997) 399.
[36] Lord Rayleigh, Philos. Mag. 34 (1892) 145.
[37] R. Bar-Ziv, E. Moses, Phys. Rev. Lett. 73 (1994) 1392.
[38] S.A. Aaronson, G.J. Todaro, J. Cell. Physiol. 42 (1968) 141.
[39] O. Thoumine, A. Ott, J. Cell Sci. 110 (1997) 2109;
J. Xu, et al., Biophys. J. 74 (1998) 2731;
H. Isambert, A. Maggs, Macromolecules 29 (1996) 1036;
F. Gittes, et al., Phys. Rev. Lett. 79 (1997) 3286.
[40] B. Geiger, Science 294 (2001) 1661.
[41] F.G. Giancotti, E. Ruoslahti, Science 285 (1999) 1028.
[42] R. Zaidel-Bar, C. Ballestrem, Z. Kam, B. Geiger, J. Cell Sci. 116 (2003) 4605.
[43] R.J. Pelham Jr., Y.-L. Wang, Proc. Natl. Acad. Sci. USA 94 (1997) 13661.
[44] C.-M. Lo, H.-B. Wang, M. Dembo, Y.-L. Wang, Biophys. J. 79 (2000) 144.
[45] D. Riveline, E. Zamir, N.Q. Balaban, U.S. Schwarz, T. Ishizaki, S. Narumiya, Z. Kam, B. Geiger, A.D. Bershadsky, J. Cell Biol. 153 (2001) 1175.
[46] A.K. Harris, P. Wild, D. Stopak, Science 208 (1980) 177;
A.K. Harris, D. Stopak, P. Wild, Nature 290 (1981) 249.
[47] G.F. Oster, J.D. Murray, A.K. Harris, J. Embryol. Exp. Morphol. 78 (1983) 83;
V.H. Barocas, R.T. Tranquillo, J. Biomech. Eng. 119 (1997) 137.

[48] M.E. Chicurel, C.S. Chen, D.E. Ingber, Curr. Opin. Cell Biol. 10 (1998) 232;
C.G. Galbraith, M. Sheetz, Curr. Opin. Cell Biol. 10 (1998) 566.
[49] K.A. Beningo, Y.-L. Wang, Trends Cell Biol. 12 (2002) 79.
[50] M. Dembo, T. Oliver, A. Ishihara, K. Jacobson, Biophys. J. 70 (1996) 2008;
M. Dembo, Y.-L. Wang, Biophys. J. 76 (1999) 2307.
[51] R. Merkel, P. Nassoy, A. Leung, K. Ritchie, E. Evans, Nature 397 (1999) 50.
[52] L.D. Landau, E.M. Lifshitz, Theory of elasticity, Pergamon, Oxford, 1970.
[53] U.S. Schwarz, N.Q. Balaban, D. Riveline, B. Geiger, S.A. Safran, Biophys. J. 83 (2002) 1380.
[54] R. Siems, Phys. Stat. Sol. 30 (1968) 645.
[55] H. Wagner, H. Horner, Adv. Phys. 23 (1974) 587.
[56] K.H. Lau, W. Kohn, Surf. Sci. 65 (1977) 607.
[57] S.A. Safran, D.R. Hamann, Phys. Rev. Lett. 42 (1979) 1410.
[58] S. Ramaswamy, J. Toner, J. Prost, Phys. Rev. Lett. 84 (2000) 3494.
[59] P. Lenz, J.-F. Joanny, F. Jülicher, J. Prost, Phys. Rev. Lett. 91 (2003) 108104.
[60] R.A. Simha, S. Ramaswamy, Phys. Rev. Lett. 89 (2002) 058101.
[61] J.P. Butler, I.M. Tolic-Norrelykke, B. Fabry, J.J. Fredberg, Am. J. Physiol. Cell Physiol. 282 (2002) C595.
[62] J.Y. Wong, A. Velasco, P. Rajagopalan, Q. Pham, Langmuir 19 (2003) 1908.
[63] F. Grinnell, Trends Cell Biol. 10 (2000) 362.
[64] P.F. Davies, A. Robotewskyj, M.L. Griem, J. Clin. Invest. 93 (1994) 2031.
[65] A. Nicolas, S.A. Safran, Phys. Rev. E 69 (2004) 051902.
[66] B.Z. Katz, E. Zamir, A.D. Bershadsky, Z. Kam, K.M. Yamada, B.B. Geiger, Mol. Cell. Biol. 11 (2000) 1047.
[67] D. Choquet, D.P. Felsenfeld, M.P. Sheetz, Cell 88 (1997) 39.
[68] B. Zimerman, B. Geiger, Double immunofluorescence of actin and vinculin shows that the density of the stress fibers decreases at the edges of the adhesion, unpublished.
[69] M. Arnold, E.A. Cavalcanti-Adam, R. Glass, J. Bluemmel, W. Eck, M. Kantlehner, H. Kessler, J. Spatz, Chem. Phys. Chem. 3 (2004) 383.
[70] A.R. Bausch, F. Ziemann, A.A. Boulbitch, K. Jacobson, E. Sackmann, Biophys. J. 75 (1998) 2038.
[71] A. Nicolas, B. Geiger, S.A. Safran, Proc. Natl. Acad. Sci. USA 101 (2004) 12520.
[72] B. Geiger, private communication.
[73] M. Kozlov, in preparation.